A Novel Gain-Enhanced Miniaturized and Lightweight Vivaldi Antenna

Ababil Hossain and Anh-Vu Pham, *Fellow, IEEE*

***Abstract*— In this article, we present the design, prototyping, and characterization of an electrically smaller ($0.36\lambda_0 \times 0.29\lambda_0 \times 0.002\lambda_0$) Vivaldi antenna with enhanced gain performance. The antenna covers a bandwidth of 450 MHz–10 GHz with an average forward realized gain of 10.82 dBi. By applying a novel technique called "cascaded cavity-based substrate cut-out (CCSC)," we were able to increase the low-frequency gain within an electrically smaller Vivaldi antenna. Because the dielectric material has been removed around cavity locations, the antenna's overall weight is reduced, giving it a high gain per unit substrate weight/volume. The high-frequency gain of the antenna has been improved with a pixelated bilayer metallic director, which flattens the antenna's overall gain profile over a wider band range. The antenna was constructed using a low-loss RT/duroid 5880 board. The measurement results match the simulation satisfactorily.**

***Index Terms*— Cavity antenna, gain-enhanced antenna, low-weight antenna, miniaturized antenna, Vivaldi antenna.**

I. Introduction

VIVALDI antennas have gained significant popularity over the years due to their wide bandwidth and high gain [1], [2]. A conventionally shaped Vivaldi antenna occupies at least a half-wavelength ($0.5\lambda_0$) in space at its lowest resonant frequency and has an average gain of 10–12 dB [3]. In an ultrawideband (UWB) system, a high gain antenna with a flat gain profile is critical; however, electrically compact antennas inherently have lower gain due to a smaller aperture area [4], [5]. This necessitates novel techniques to attain higher flat gain in an electrically compact Vivaldi antenna.

In a traditional antenna, current path elongation in the aperture helps to accommodate a longer electrical length. This scales down the lowest resonant frequency, and in the process, renders size miniaturization. In this miniaturization method, the antenna's gain reduces due to phase cancellation at different portions of the antenna structure. Following this type of principle in [6], an L-shaped slot in the Vivaldi radiating fin reduces the antenna size by around 28%, producing a gain in the range of 1.8–6.9 dB. In [7], another electrically compact Vivaldi antenna is presented where a reduced low-frequency gain still remains a prime concern. Another popular method of attaining electrical compactness is using lumped component loading, such as resistors, inductors, and capacitors. This can scale down the lower resonant frequency of a Vivaldi antenna by improving matching in the antenna network. Specifically, resistor-loaded Vivaldi antennas can have significantly reduced size by up to 50%, yet the average gain is even lower in the range of 0.9–7.8 dB [8]. Recently, in [9], Saleh et al. developed a miniaturized planar Vivaldi antenna by using nonuniform transmission line theory. The size of the antenna was reduced by greater than 50% while achieving a substantial level of gain improvement in its mid-band frequency range. Despite this, the application of nonuniform transmission line theory does not improve low-frequency gain, which negatively impacts the overall gain flatness of the antenna.

To compensate for the inherently reduced gain associated with an antenna having a smaller aperture, the localized surface current density in the radiator needs to be enhanced. To meet this need, Vivaldi designs using tapered slots [10], resonant cavity structures [11], etc., have shown excellent promise in literature. Applying these techniques increases the low-frequency gain while keeping the antenna size reduced, yet at mid-band frequency ranges the gain becomes less flat. By incorporating additional resonant structures or metamaterials in the antenna, the gain can be enhanced as well, but within a very narrow-band range [12], [13]. Increased width also enhances the gain of the Vivaldi antenna due to the increase in the aperture area. Similarly, a double-slotted Vivaldi has been reported in [14] where two feeding slots used in the same antenna improve gain. Some other novel techniques for gain enhancement that have been described in the literature include dielectric loading [15], [16], dielectric substrate shaping [17], and parasitic patch [18]. While these techniques increase antenna gain mainly at higher frequency bands, they also increase both the antenna size and fabrication complexity. Therefore, designing a compact Vivaldi antenna with enhanced gain along with a flatter gain profile in a wideband range remains a very challenging task.

Vivaldi antennas have been modified with the substrate cut-out technique to improve the high-frequency gain and correct pattern tilt [19]. Additionally, designers can carve dielectric-shaped grooves within a Vivaldi antenna to narrow the beamwidth and improve the front-to-back ratio [20].

Manuscript received 20 April 2023; revised 12 August 2023; accepted 23 August 2023. Date of publication 6 September 2023; date of current version 20 December 2023. This work was supported by the Department of the Navy, Office of Naval Research, under Award N00014-22-1-2167. Any opinions, findings, and conclusions or recommendations expressed in this material are those of author(s) and do not necessarily reflect the views of the Office of Naval Research. *(Corresponding author: Ababil Hossain.)*

The authors are with the Department of Electrical and Computer Engineering, University of California at Davis, Davis, CA 95616 USA (e-mail: mahossain@ucdavis.edu; pham@ece.ucdavis.edu).

Color versions of one or more figures in this article are available at https://doi.org/10.1109/TAP.2023.3310611.

Digital Object Identifier 10.1109/TAP.2023.3310611

TABLE I
GEOMETRICAL PARAMETERS OF THE OPTIMIZED ANTENNA

Parameter	Value (mm)	Parameter	Value (mm)
L	244.16	Sw1	3.2
W	195	Sw2	3.4
d1	23	Sw3	8
d2	20	Sg	1.8
d3	23	Dl	104
θ	60°	Hr	6
Cl	9.5	Hg	11.8
Cw	1.8	Pl	6
Cg	1.8	Pw	2
Bl	14.8	Pg	2
Bw	54		

Nevertheless, these techniques do not affect the overall current density because the metallic portion of the antenna radiator remains completely unaffected. As a result, these techniques do not contribute to significant enhancement of the low-frequency gain, which is extremely important in UWB communications.

In this article, we present the design, development, and experimental verification of a miniaturized and low-weight Vivaldi antenna with enhanced gain performance over wide frequency bandwidth. The antenna attains around 40% size miniaturization, 2–3 dB of increased low-frequency gain, and about 20% reduction in overall weight compared to a similar-sized conventional Vivaldi antenna. A novel "cascaded cavity-based substrate cut-out (CCSC)" technique has been applied to attain low-frequency gain enhancement within an electrically compact structure, while a pixelated bilayer metallic director improves high-frequency gain without increasing the overall size of the antenna. Enhancement of low-frequency and high-frequency gain makes the antenna's gain profile flatter, allowing pulse transmission with low distortion and high fidelity.

II. DEVELOPMENT OF CAVITY-BASED VIVALDI ANTENNA

A. Overview of the Cavity-Based Vivaldi Antenna

Fig. 1 displays the antenna schematic with the necessary symbols, whilst Table I lists the dimensional parameters with numerical values. In Fig. 1, multiple cascaded cavity structures (CCS), a pixelated bilayer director, and two absorbers have been incorporated into a Vivaldi antenna. A cascaded cavity structure enhances low-frequency gain by concentrating higher current density around its periphery. An individual cascaded cavity structure is formed by placing several circular cavities in tandem. Each circular cavity has a diameter of 12 mm, and the centers of two neighboring cavities are separated by 11.8 mm. As seen from Fig. 1, five rows of cascaded cavity structures (denoted by CCS#1–5) are symmetrically placed on both arms. The tapered profile of CCS#1 follows the original taper of the main antenna (Curve C1) to accommodate a maximum number of cavity holes for enhanced size miniaturization. The remaining cascaded cavity structures (CCS#2–5) have relatively straighter shape profiles and are designed based on the current distributions on the antenna surface. They are placed in parallel with CCS#1 at an angle of 60° with the horizontal X-axis. During the printed circuit board (PCB)

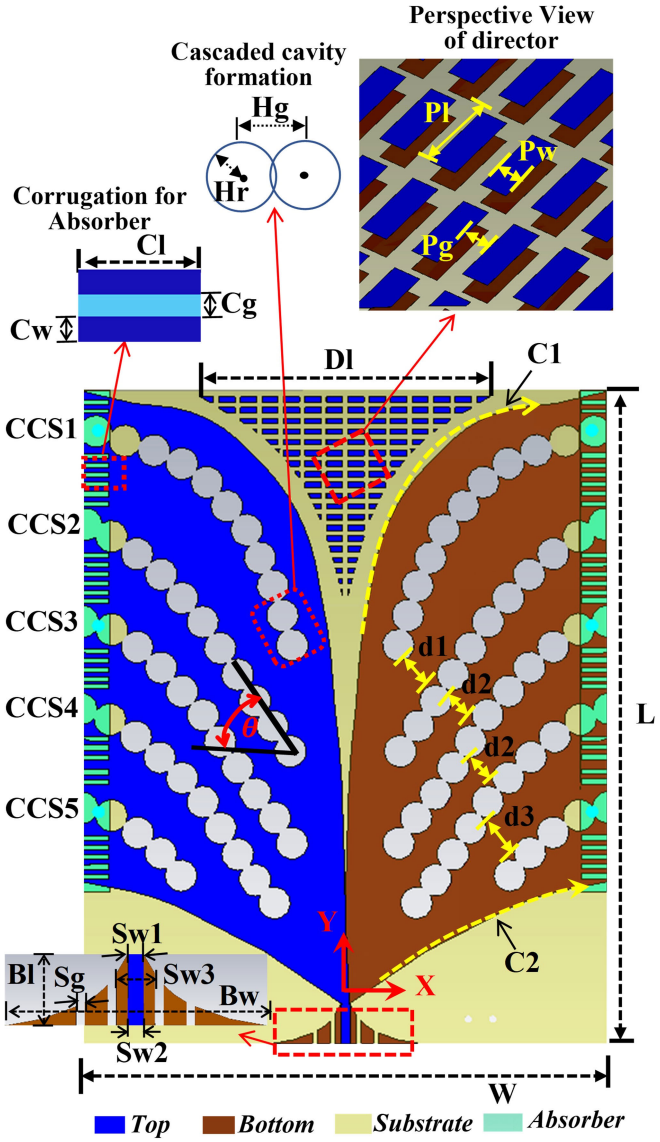

Fig. 1. Schematic of Cavity Vivaldi Antenna with necessary dimensions.

fabrication process, the dielectric material beneath each cavity is milled out. Importantly, the dielectric portion under the last two cavity holes in a cascaded cavity structure is not cut out to maintain the mechanical support. The start and end taper of the original Vivaldi arm can be represented by the following two curves in (1) and (2), where W is the antenna width.

$$\text{C1: } y = \frac{234.3x}{4.63 + x} \text{ mm}, \quad 0 \le x \le \frac{W}{2} \tag{1}$$

$$\text{C2: } y = 90 - 90e^{-0.008x} \text{ mm}, \quad 0 \le x \le \frac{W}{2}. \tag{2}$$

Among the other major components of the antenna, as seen in Fig. 1, a taper-shaped metallic director is deployed in the open space near the radiating slot line aperture. The director is a bilayer structure that consists of small segmented rectangular metallic pixels, illustrated in the perspective view of Fig. 1. The director enhances the high-frequency gain without any further size increase of the antenna. Additionally, a microwave absorbing materials (MAMs) layer is placed on the sides of

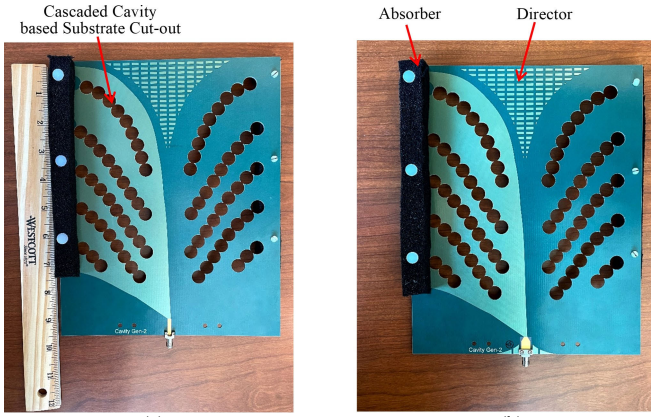

Fig. 2. Fabricated prototype of Cavity Vivaldi. (Note: absorbers are placed antipodally on both sides.) (a) Top view. (b) Bottom view.

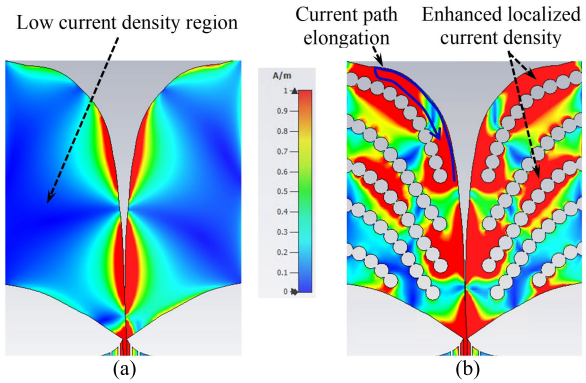

Fig. 3. Surface current density comparison of a typical antipodal Vivaldi versus cavity-array-based Vivaldi at 1.5 GHz. (a) Conventional Vivaldi. (b) Cavity-array-based Vivaldi.

TABLE II
COMPARISON OF ANTENNA PERFORMANCE PARAMETERS

Antenna Types	*Avg. Realized Gain*	*Lower cut-off frequency*	*Weight*
Traditional Vivaldi	9.79 dB	750 MHz	180 g (approx.)
Cavity Vivaldi	10.82 dB	450 MHz	151 g (measured)

each cascaded cavity structure to alleviate ripples in return loss and gain due to current resonance. The Vivaldi is fed with a tapered balun, with two parallel slots cut on both sides of the ground. The parallel slots enhance the balun current's odd mode component, improving phase balance at the output.

The design flow of the cavity antenna can be summarized in the following three steps:

Step 1: We optimized the size, shape, and position of the CCS.

Step 2: We selected an absorber material in the operating frequency range and placed it upon the open cavity terminals in order to alleviate the transient effects of cavity structures on return loss and gain.

Step 3: We optimized the length, width, and gap of the unit element of the bilayer pixelated metallic director so the $\pm 90^{\circ}$ reflection phase bandwidth of the unit pixel would cover the antenna's higher edge of the bandwidth.

A prototype of the antenna was fabricated with a low-loss RT/duroid 5880 substrate ($\epsilon_r = 2.2$, $tan\delta = 0.0085$) having a thickness of 1.57 mm. Fig. 2 presents the top and bottom view of the novel cavity Vivaldi antenna with its main distinguishing features marked.

In Table II, the performance metrics of our designed cavity Vivaldi are compared with those of a conventional antipodal Vivaldi of the same size. This demonstrates that the cavity Vivaldi antenna has better gain, size, and weight.

B. Cavity Array

A conventional Vivaldi is a resonant antenna at low frequency, where its surface current density is mainly concentrated around the edges of the arm. There is significantly less current in the middle, which means that there is a very minimal contribution from this portion to the overall radiation performance of the antenna [seen in Fig. 3(a)]. Hence if the localized current density in the middle portion of a Vivaldi antenna can be enhanced, it can increase the magnetic field intensity of the Poynting vector, thus causing the gain to increase significantly. For our cavity Vivaldi, electric charges are accumulated around the metallic CCS at sharp edges where the repulsive force between the same polarity charges is minimal. This enhances charge density around the periphery of the CCS and subsequently enhances localized current density, as shown in Fig. 3(b).

Using characteristic mode theory (CMT), we have determined that the presence of cavities in the antenna enhances the surface current density of the desired odd modes with strong current resonance, while suppressing even mode current more prominently [21], [22], [23]. According to CMT, the total current density on the antenna surface can be expressed as the linear superposition of the modal currents, i.e., $\mathcal{J} = \sum_n \alpha_n \boldsymbol{J_n}$.

To demonstrate an example of this, we ran a CMT analysis for the first ten modes in CST. Fig. 4 compares the corresponding current density and patterns for two different modes at 1.5 GHz in the cavity antenna. As evident from Fig. 4(a), mode-3 is an even mode with its current ($\mathbf{J_3}$) spread throughout the antenna surface, causing undesirable broadside radiation. By comparison, mode-8 has its current ($\mathbf{J_8}$) concentrated on the cavity edges, with the current distribution resembling an odd mode. This causes directive patterns in the endfire direction.

Five rows of CCS boost the low-frequency gain. Every cascaded cavity structure is essentially an open-slotted metallic structure, so a current loop is not formed around its periphery. A current loop distorts the odd mode current distribution on the Vivaldi aperture, distorting the endfire radiation from the antenna. Size miniaturization has been attained through current path elongation near the radiating aperture, displayed previously in Fig. 3(b). Furthermore, the overall weight of the antenna reduces due to substrates being cut out underneath the CCS. Therefore, in incorporating the cavity array, we present a unified approach to simultaneously achieving low-frequency

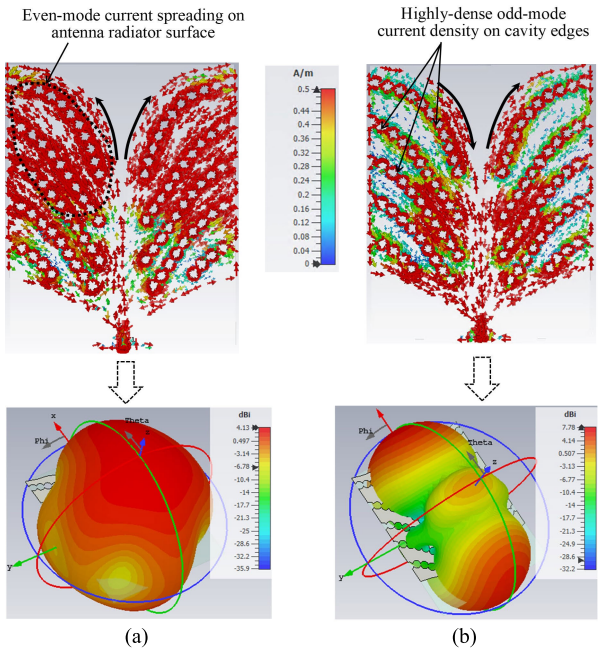

Fig. 4. Characteristic mode analysis at 1.5 GHz with corresponding current density and directivity for different modes. (a) Mode-3 (even mode). (b) Mode-8 (odd mode).

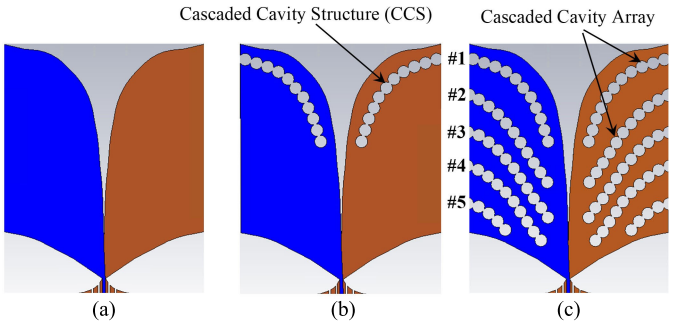

Fig. 5. Vivaldi with different combinations of cascaded cavity structures (CCS). (a) Traditional antipodal Vivaldi. (b) Vivaldi with one row of CCS. (c) Vivaldi with five rows of CCS.

gain enhancement, antenna miniaturization, and weight reduction.

1) Analysis of Cavity Arrays on Antenna Gain and Lower Cut-Off Frequency: To analyze the exact effect of cavities, we simulate different configurations of Vivaldi in CST Microwave Studio software, as shown in Fig. 5. Displayed are the traditional antipodal Vivaldi, a Vivaldi with one row of cascaded cavity structure, and a Vivaldi with five rows of CCS. The antennas are simulated without any absorber to accurately observe the cavity structures' effect.

Fig. 6 demonstrates the effects of cavities on the gain and return loss. As evident from Fig. 6(a), a cavity-based Vivaldi exhibits superiority in gain compared to a traditional antipodal Vivaldi. With one row of CCS, gain enhancement is achieved only at a lower frequency near 0.5 GHz compared to a simple or conventional Vivaldi antenna of the same size. A Vivaldi with two rows of cavities (#1 and #2) exhibits a significant increase in gain in the low-frequency region,

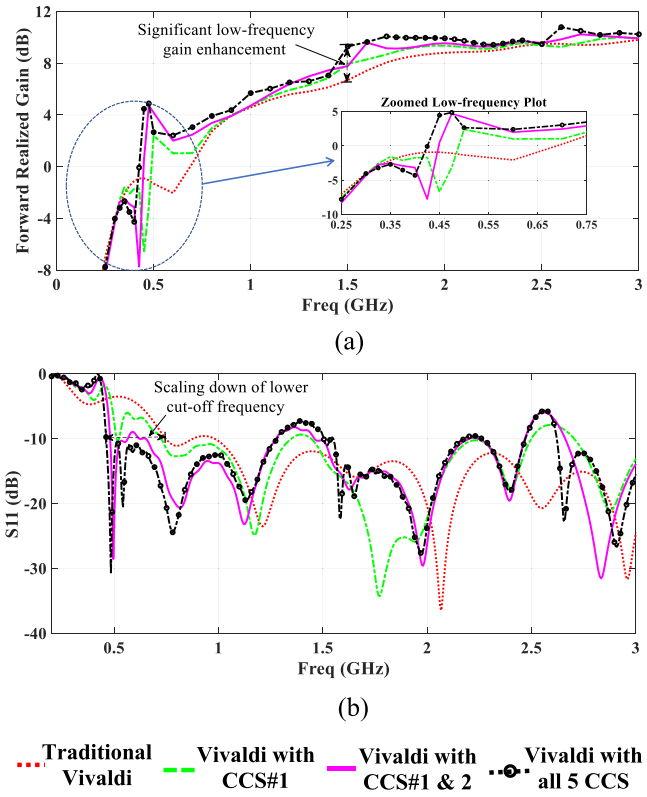

Fig. 6. Simulated (a) low-frequency gain and (b) reflection co-efficient comparison for a different number of rows of cavity structures.

up to almost 3 GHz. For additional cavity rows, although the increase in gain is subtle, the gain curve gradually flattens in the low-frequency region. With five rows of CCS, a gain increase of around 2.5–3 dB over a wider bandwidth is achieved; the gain at the lower edge of the band at 450 MHz is 4.47 dB. This happens because current resonates on each cascaded cavity structure when the length of the cavity row is comparable to $\lambda/4$, $\lambda/2$, λ, and so on. In our design, resonance occurs at 0.5, 1.5, and 2.6 GHz as evident from the gain in Fig. 6(a). At these frequencies, the length of one row of cavities becomes comparable to a multiple of a quarter-wavelength. A significant current and gain enhancement occurs when the length of a cavity row is about $\lambda/2$ (full-wave dipole) in its electrical length, which happens near 1.5 GHz in our design. At this frequency, the length of the first four longer cavity rows (CCS#1–4) on each side becomes comparable to a half-wavelength. Based on classical array theory, the cavities work like a dipole array, where each cascaded cavity structure works as a unit antenna element of the array. The distance between two elements in the cavity array is almost the same, which ensures a constant phase difference ($\alpha = \beta d$) between individual array elements since they are excited by the same flared transmission line from the antenna port [24]. Theoretically, the array factor is maximized toward the endfire direction to enhance the gain. The result is an enhanced low-frequency gain up to almost 3 GHz. After 3 GHz, the traveling wave radiation mode of the Vivaldi dominates when the radiation occurs mainly from the slot line aperture, similar to a traditional Vivaldi antenna. Due to this, the effects of

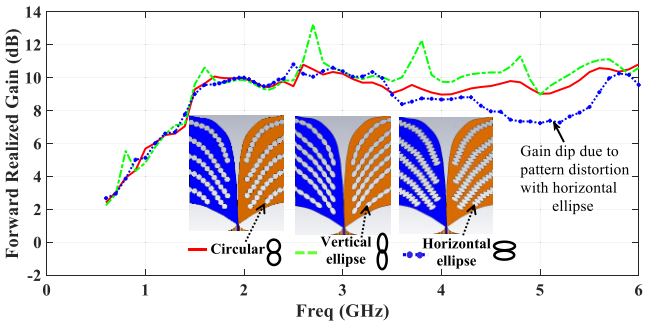

Fig. 7. Simulated forward realized gain comparison for different shapes of cascaded cavity structure (without MAMs).

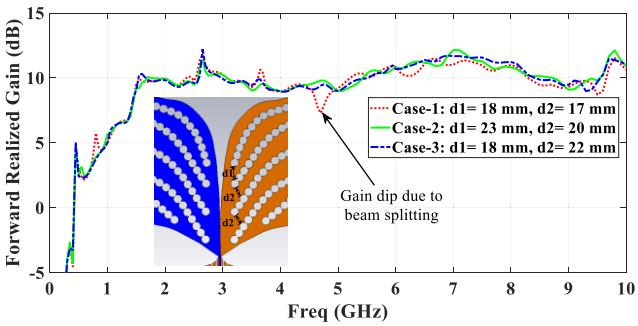

Fig. 8. Simulated forward realized gain for different interelement distances in cavity array.

cavity arrays on gain enhancement are minimal at higher frequencies.

A traditional Vivaldi has an electrical length of around $\lambda/2$, where λ is the wavelength corresponding to the lowest operating frequency. The cascaded cavity structure elongates the current path in the antenna aperture, explained earlier in Fig. 3(b). This accommodates a larger electrical length in the antenna, causing the antenna to resonate at a lower frequency. The phenomenon of frequency getting scaled-down is explained in Fig. 6(b). The traditional Vivaldi has a cut-off frequency with a reflection coefficient of -10 dB at 750 MHz. Due to the addition of the first row of cavities, the cut-off frequency scales down to 510 MHz. With two rows of cavities (#1 and #2), the lower cut-off frequency reduces to 480 MHz due to the mutual coupling between adjacent CCS. Additional cavity rows gradually reduce the resonant frequency. When five rows of cavities are used, the lower cut-off frequency shifts down to 460 MHz, achieving a $\sim$38% reduced size antenna compared to a traditional Vivaldi of the same size.

2) Optimization Analysis of Cavity Arrays: To achieve the best radiation performance from the antenna, it is necessary to optimize the interelement spacing between two adjacent rows of cavity structures and the geometry of the unit cavity in CCS. During the optimization process, gain enhancement in the endfire direction is given the utmost priority. Originally, we started from a simple conventional antipodal Vivaldi antenna having a lower cut-off frequency of 750 MHz. We then deployed, modified, and optimized the shape and location of the five rows of cavity structures in the antenna.

a) Size and shape of the cavity unit: Different shaped cavity units are applied to form a cascaded cavity structure. Circular cavity, vertical, and horizontal elliptical-shaped cavities are among those contained in the inset of Fig. 7. We then compare the forward realized simulated gain for different shapes of the cavity in Fig. 7. Evidently, both circular (red) and vertical elliptical (green) shaped cavities yield enhanced gain performance with a flatter gain profile. Simulation reveals that the vertical elliptical cavity unit offers somewhat superior gain improvement over the circular unit because of its ability to guide secondary traveling wave branches at higher frequencies. However, considering PCB requirements, we choose a circular cavity shape for fabrication compatibility where the diameter of the circular cavity is 12 mm to optimize gain performance. It is also noticeable that the horizontal elliptical cavity shape (blue) causes severe standing waves at higher frequencies. Because of this, beam splitting occurs, causing side lobes to appear in the radiation pattern and lowering forward or endfire gain. Therefore, this design does not employ the horizontal elliptical-shaped cavity unit.

b) Interelement distance between cascaded cavity structures: For CCS to achieve an improved gain in the endfire direction, optimum interelement spacing is crucial. Fig. 8 explains the effect of interelement spacing. Strong mutual coupling causes the peripheral current and electric field distribution of closely spaced cavity structures to be distorted. This results in severe beam splitting and pattern distortion at various frequencies, causing forward realized gain to reduce. The 4.7 GHz frequency illustrates this in Fig. 8 (Case-1). In the inset, the distances $d1$ and $d2$ are marked.

In Fig. 9, the beam-splitting phenomenon at 4.7 GHz is illustrated with electric field distribution on the cavity structures and the corresponding 3-D radiation patterns. As seen in Fig. 9(a), when cavity rows are closely spaced strong mutual coupling between adjacent cavity rows distorts the E-field pattern, causing the beam-splitting effect. However, in the case of optimally spaced cavity rows as in Fig. 9(b), the E-field pattern around the individual cavity rows is mostly unaffected; hence no beam-splitting occurs. Considering the flatness of gain, the optimum distances for $d1$ and $d2$ are chosen at 23 and 20 mm, respectively (Case-2 in Fig. 8).

C. Microwave Absorbing Materials (MAMs)

MAMs have been used on metallic corrugation on either side of the cavity Vivaldi antenna. Our MAM is Eccosorb-AN79 which has a high absorption property, reflecting less than -17 dB of normal incident energy in the 0.5–20 GHz range [25]. MAMs function as a matched impedance layer for RF frequency absorption. In doing so, it lessens the standing wave effect caused by reflection from the open cascaded cavity terminals. Fig. 10 shows the simulated return losses of the cavity Vivaldi with and without MAMs. With MAMs, the return loss parameter is significantly enhanced, especially at lower frequencies. Without MAMs, transient effects in the cavities cause unwanted spikes in the return loss deteriorating the UWB performance of the antenna.

D. Pixelated Bilayer Metallic Director

We design a bilayer director composed of small optimized rectangular metallic pixels for high-frequency gain enhancement. As previously shown in the schematic design of Fig. 1,

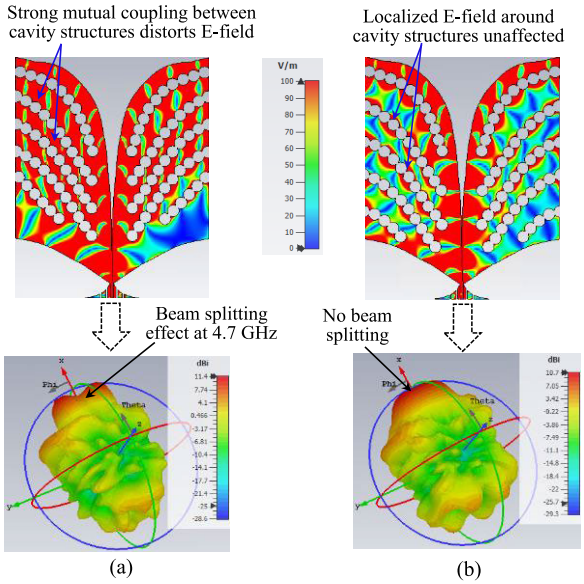

Fig. 9. Electric field distribution and corresponding beam splitting phenomenon at 4.7 GHz. (a) Closely spaced cavity rows ($d1 = 18$ mm, $d2 = 17$ mm). (b) Optimally spaced cavity rows ($d1 = 23$ mm, $d2 = 20$ mm).

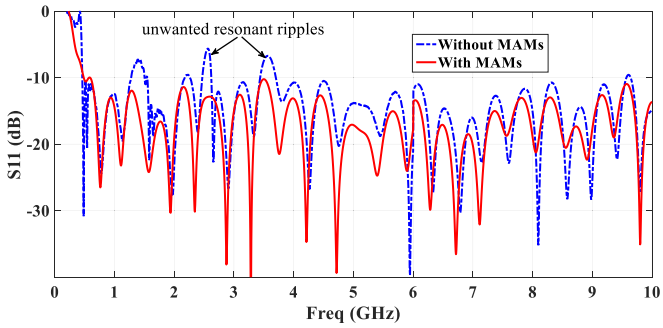

Fig. 10. Simulated return losses of the cavity antenna with and without MAMs.

the pixels are positioned periodically in 2-D space to create a taper-shaped structure within the main antenna radiating slot. The designed director is both broadband and highly compact.

1) Design Principle: The basic working principle of our director is similar to a high-impedance surface [26], [27], [28], [29]. To investigate the director's accurate impedance and scattering profile, we run a Floquet port analysis of a unit cell from the bilayer pixelated structure in Ansys HFSS, as seen in the setup of Fig. 11(a). The unit cell comprises a top and bottom pixel on the central substrate. The substrate has the same thickness and properties as the original antenna. The unit cell is excited with a plane wave (TE_{00} mode) by a Floquet port from the top; primary and secondary boundary pairs are assigned on the four sides, making it infinite in the 2-D transverse direction in simulation. We categorized the pixels into three groups based on their dimensions: Type-I is more compact, whereas Type-III is longer, shown in Fig. 11(b).

The impedance profile of the pixelated bilayer structure varies depending on the frequency of the incident plane waves. As evident from Fig. 12(a), at lower and higher frequencies the impedance magnitude of the pixelated structure is very low. However, the impedance abruptly increases at the resonant

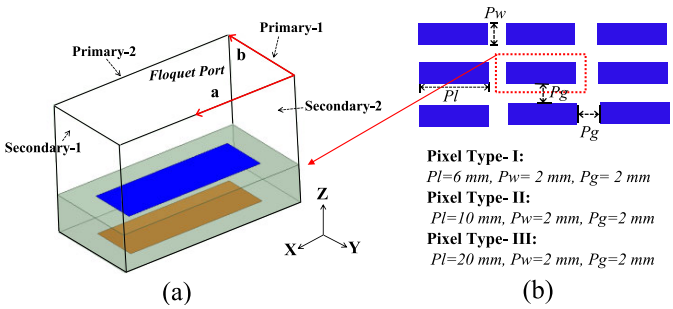

Fig. 11. (a) Unit cell simulation set-up in Ansys HFSS and (b) dimensional specifications of bilayer metallic pixelated structure.

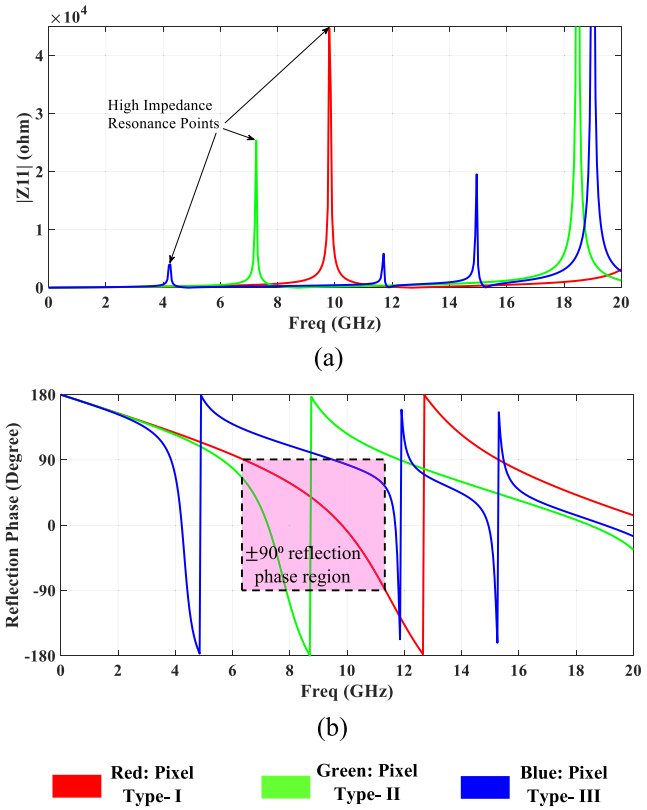

Fig. 12. (a) Magnitude of Z11 and (b) reflection phase ($\angle S11$) variation for different pixel types.

frequency, much like in a high-impedance surface or perfect magnetic conductor (PMC). The frequency where the peak impedance occurs also changes for different pixel dimensions. We see that the resonant frequency shifts from 9.8 to 4.25 GHz when the length of the metallic segment increases (Pixel Type-III from Pixel Type-I).

The reflection phase of the pixelated structure is represented in Fig. 12(b). At very low frequencies, the pixelated structure has a reflection phase close to 180°, making it work like a perfect electric conductor (PEC), while at the resonant frequency the reflection phase is 0°. The frequency region with ±90° reflection phase is the frequency region where the phase of the incident electric field is not reversed during reflection. This is one of the most critical properties of a high-impedance PMC surface, which has been frequently utilized to improve

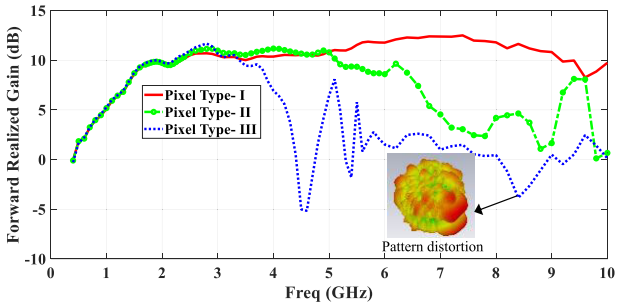

Fig. 13. Simulated forward realized gain comparison for different pixel types in the director.

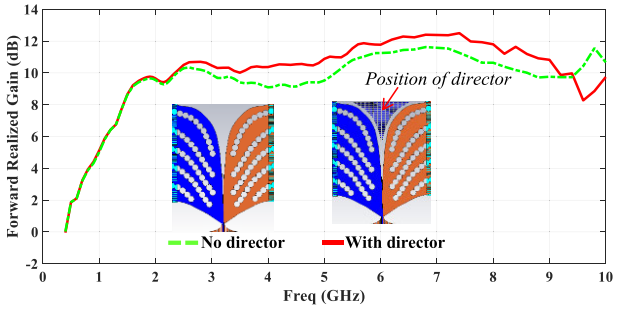

Fig. 14. Simulated forward realized gain comparison with and without a director.

antenna radiation performance over the decades. As per the conditions of the PMC surface, at the resonant frequency the magnetic field is zero on the interface, while the amplitude of the electric field reaches the maximum. The enhanced induced electric field within the ±90° reflection phase bandwidth enhances the antenna's average radiated power and endfire gain. The reflection phase plot in Fig. 12(b) demonstrates that the reflection phase bandwidth region can also be tuned by changing the pixel dimension. Pixel Type-I's reflection phase bandwidth is marked pink in the shaded portion.

2) Parametric Analysis of Pixel Type in Director: Parametric analysis was run for different pixel dimensions within the tapered pixelated director. The pixel unit length controls the inductance of the pixelated structure, and the interpixel gap controls its capacitance value. For the convenience of illustration, we only vary the length of an individual pixel and keep the other two parameters (width and interpixel gap) fixed. The exact dimensions of different pixel types have been shown previously in Fig. 11. We investigated the gain profiles for the types (Type-I to Type-III) in the antenna's director, displayed in Fig. 13. Pixel Type-I has a shorter length and yields a flatter gain profile, while Pixel Type-III evinces reduced gain bandwidth. In fact, partial reflection of the incoming wave starts to originate due to longer length in Pixel Type-III after 3.1 GHz. This distorts the original radiation patterns emanating from the slot line aperture region, reducing the forward gain. To maintain UWB gain performance close to 10 GHz, optimum pixel length, width, and gap values are chosen at 6, 2, and 2 mm, respectively (Pixel Type- I).

3) Gain Enhancement in Cavity Antenna With Director: A taper-shaped metallic director composed of the pixelated bilayer structure is deployed in the vacant space of slot line aperture shown in the inset of Fig. 14. When the frequency of the incident wave from the main radiator antenna falls within the reflection phase bandwidth of the pixelated bilayer director, it is transmitted with enhanced magnitude. The overall result is an enhanced gain of around 1.5–2 dB in the frequency band from 2.5–9 GHz, demonstrated in Fig. 14. Outside the reflection phase bandwidth region, the forward or endfire gain eventually starts to fall due to beam splitting or pattern distortion, as evident near 9.7 GHz in Fig. 14.

III. Measurement Results

The return loss of the cavity Vivaldi was measured, which demonstrates satisfactory matching with the simulation,

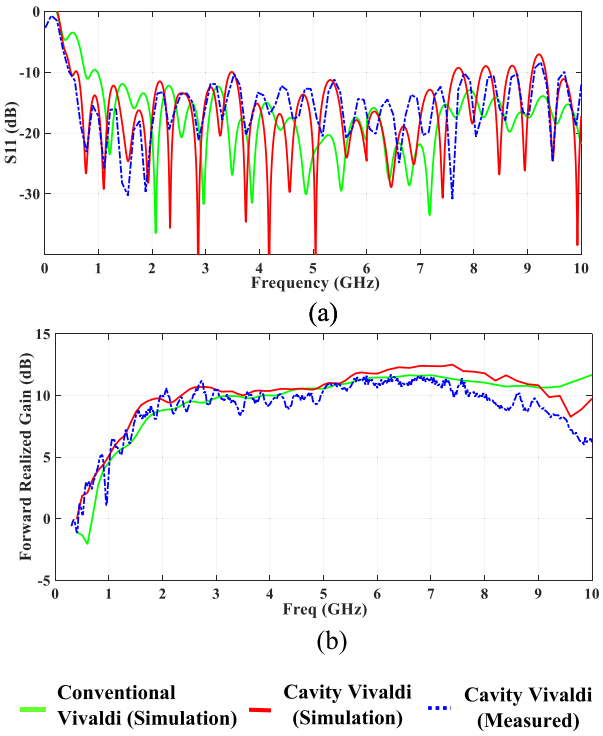

Fig. 15. Comparison of (a) return loss and (b) gain of cavity Vivaldi with a conventional Vivaldi of the same size.

as shown in Fig. 15(a). The green curve is the simulated return loss of a conventional antipodal Vivaldi of the same size.

The novel cavity array-based Vivaldi has a lower cut-off frequency than the conventional one. As also evident from Fig. 15(a), the cavity antenna produces close to 10 dB measured return loss from 450 MHz to 10 GHz. There are small ripples of around −8 dB in the S11 near 9.25 GHz, which is within the tolerable limit. The forward realized gain is compared in Fig. 15(b), where the cavity Vivaldi antenna exhibits enhanced gain compared to a similar-sized antipodal Vivaldi, almost up to 9 GHz. It is also seen that the gain curve remains relatively flat over the UWB range from 1.8 to 9 GHz.

The radiation patterns were measured in the anechoic chamber, which are plotted and compared with simulation data at both E and H planes in Fig. 16. The simulated and measured data of the radiation patterns show satisfactory matching, although the measured gain is around 1 dB less compared to simulation.

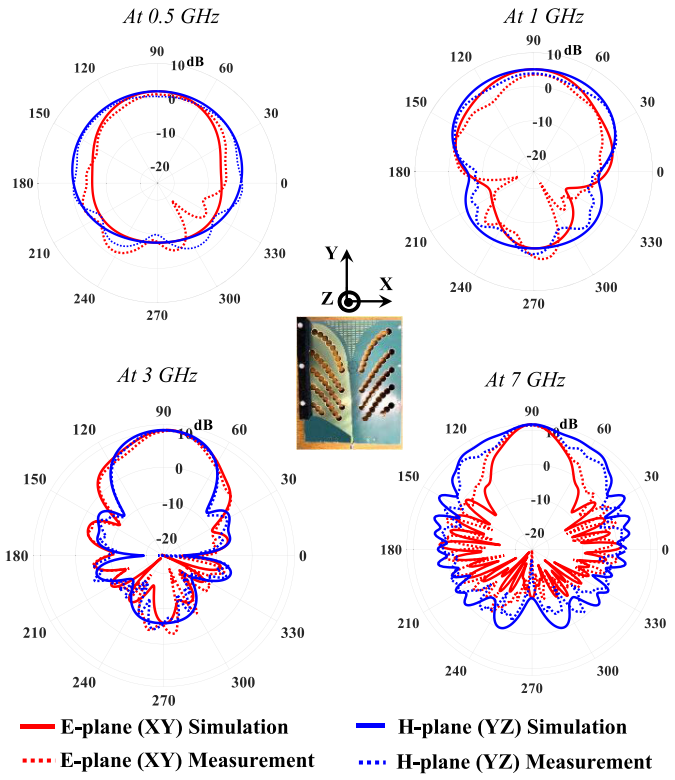

Fig. 16. Comparison of simulated and measured value of 2-D radiation patterns of the cavity Vivaldi.

TABLE III
COMPARISON BETWEEN PROPOSED ANTENNA AND LITERATURE

Ref. no.	Lateral Dimension	-10 dB S11 Bandwidth	Avg. Re. Gain	FOM
[10]	$0.48\lambda_0 \times 0.38\lambda_0$	2.4- 14 GHz	7.51 dB	30.9
[11]	$0.43\lambda_0 \times 0.25\lambda_0$	0.5-6 GHz	5.02 dB	29.55
[13]	$1.17\lambda_0 \times 0.67\lambda_0$	2.5-13.5 GHz	10.65 dB	14.82
[14]	$1.25\lambda_0 \times 0.67\lambda_0$	2.5-15 GHz	11.57 dB	17.14
This Paper	*$0.36\lambda_0 \times 0.29\lambda_0$*	*0.45-10 GHz*	*10.82 dB*	*115.7*

Table III compares our designed cavity Vivaldi antenna in terms of size, bandwidth, and gain with the literature. It is evident that the designed cavity Vivaldi establishes a higher figure of merit (FOM) than any other antenna. Here, FOM is defined in (3) by the respective antenna's liner average realized gain divided by its normalized area expressed in terms of λ_0, where λ_0 is the wavelength in free space corresponding to the lowest resonance frequency

$$\text{FOM} = \frac{\text{Average Re. Gain}}{\text{Normalized Area}}. \tag{3}$$

In the cavity-based Vivaldi antenna, the cascaded cavity structure condenses strong currents around the edges when shaped in a circular or vertical ellipse, enhancing the low-frequency gain. The gain also does not decrease drastically after the initial increase due to multiple resonances within the low-frequency region, which is distinct from other methods, such as tapered slots [10], [11]. This ensures an enhanced flat gain at the lower end of the band. Furthermore, using a pixelated director with a broadband high-impedance surface enhances the E-field near the radiating slot-line aperture at the higher end of the band. This allows for gain enhancement at higher frequencies, which consequently flattens the overall gain profile. In addition to these gain enhancements, current path elongation and subsequent mutual coupling in the cavity rows cause the lower resonant frequency to scale down, significantly reducing the antenna's electrical size. The overall result is a higher average gain within a compact antenna architecture.

IV. CONCLUSION

A gain-enhanced modified Vivaldi antenna with compact size and lightweight performance has been designed and fabricated based on the novel cascaded cavity-based substrate cut-out technique. The antenna achieves a 40% reduction in size, a 2–3 dB boost in low-frequency gain, and a 20% reduction in overall weight compared to a conventional antipodal Vivaldi antenna of the same size. The circular-shaped cavity enhances low-frequency gain, while a pixelated bilayer metallic director enhances high-frequency gain, flattening the gain profile over a broadband range. Absorbers on the sides help reduce return loss ripples in addition to improving pattern characteristics. The fabricated antenna prototype shows satisfactory matching with the simulated model in terms of return loss and gain performance.

REFERENCES

[1] P. J. Gibson, "The Vivaldi Aerial," in *Proc. 9th Eur. Microw. Conf.*, Brighton, U.K., Jun. 1979, pp. 101–105.

[2] D. Schaubert, E. Kollberg, T. Korzeniowski, T. Thungren, J. Johansson, and K. Yngvesson, "Endfire tapered slot antennas on dielectric substrates," *IEEE Trans. Antennas Propag.*, vol. AP-33, no. 12, pp. 1392–1400, Dec. 1985.

[3] C. B. Hien, H. Shirai, and D. N. Chien, "Analysis and design of antipodal Vivaldi antenna for UWB applications," in *Proc. IEEE 5th Int. Conf. Commun. Electron. (ICCE)*, Jul. 2014, pp. 391–394.

[4] H. A. Wheeler, "Fundamental limitations of small antennas," *Proc. IRE*, vol. 35, no. 12, pp. 1479–1484, Dec. 1947.

[5] H. Wheeler, "Small antennas," *IEEE Trans. Antennas Propag.*, vol. AP-23, no. 4, pp. 462–469, Jul. 1975.

[6] R. Natarajan, J. V. George, M. Kanagasabai, and A. K. Shrivastav, "A compact antipodal Vivaldi antenna for UWB applications," *IEEE Antennas Wireless Propag. Lett.*, vol. 14, pp. 1557–1560, 2015.

[7] A. Z. Hood, T. Karacolak, and E. Topsakal, "A small antipodal Vivaldi antenna for ultrawide-band applications," *IEEE Antennas Wireless Propag. Lett.*, vol. 7, pp. 656–660, 2008.

[8] C. Deng and Y.-J. Xie, "Design of resistive loading Vivaldi antenna," *IEEE Antennas Wireless Propag. Lett.*, vol. 8, pp. 240–243, 2009.

[9] S. Saleh, W. Ismail, I. S. Z. Abidin, M. H. Jamaluddin, M. H. Bataineh, and A. S. Al-Zoubi, "Novel compact UWB Vivaldi nonuniform slot antenna with enhanced bandwidth," *IEEE Trans. Antennas Propag.*, vol. 70, no. 8, pp. 6592–6603, Aug. 2022.

[10] P. Fei, Y.-C. Jiao, W. Hu, and F.-S. Zhang, "A miniaturized antipodal Vivaldi antenna with improved radiation characteristics," *IEEE Antennas Wireless Propag. Lett.*, vol. 10, pp. 127–130, 2011.

[11] Y. Liu, W. Zhou, S. Yang, W. Li, P. Li, and S. Yang, "A novel miniaturized Vivaldi antenna using tapered slot edge with resonant cavity structure for ultrawideband applications," *IEEE Antennas Wireless Propag. Lett.*, vol. 15, pp. 1881–1884, 2016.

[12] R.-C. Deng et al., "Performance enhancement of novel antipodal Vivaldi antenna with irregular spacing distance slots and modified-w-shaped metamaterial loading," *Appl. Phys. A, Solids Surf.*, vol. 125, p. 5, Dec. 2018.

[13] B. Zhou and T. J. Cui, "Directivity enhancement to Vivaldi antennas using compactly anisotropic zero-index metamaterials," *IEEE Antennas Wireless Propag. Lett.*, vol. 10, pp. 326–329, 2011.

[14] Y.-W. Wang, G.-M. Wang, and B.-F. Zong, "Directivity improvement of Vivaldi antenna using double-slot structure," *IEEE Antennas Wireless Propag. Lett.*, vol. 12, pp. 1380–1383, 2013.

[15] J. Bourqui, M. Okoniewski, and E. C. Fear, "Balanced antipodal Vivaldi antenna with dielectric director for near-field microwave imaging," *IEEE Trans. Antennas Propag.*, vol. 58, no. 7, pp. 2318–2326, Jul. 2010.

[16] R. Cicchetti, V. Cicchetti, A. Faraone, L. Foged, and O. Testa, "A compact high-gain wideband lens Vivaldi antenna for wireless communications and through-the-wall imaging," *IEEE Trans. Antennas Propag.*, vol. 69, no. 6, pp. 3177–3192, Jun. 2021.

[17] M. Moosazadeh, S. Kharkovsky, J. T. Case, and B. Samali, "Improved radiation characteristics of small antipodal Vivaldi antenna for microwave and millimeter-wave imaging applications," *IEEE Antennas Wireless Propag. Lett.*, vol. 16, pp. 1961–1964, 2017.

[18] I. T. Nassar and T. M. Weller, "A novel method for improving antipodal Vivaldi antenna performance," *IEEE Trans. Antennas Propag.*, vol. 63, no. 7, pp. 3321–3324, Jul. 2015.

[19] N.-N. Wang, M. Fang, H.-T. Chou, J.-R. Qi, and L.-Y. Xiao, "Balanced antipodal Vivaldi antenna with asymmetric substrate cutout and dual-scale slotted edges for ultrawideband operation at millimeter-wave frequencies," *IEEE Trans. Antennas Propag.*, vol. 66, no. 7, pp. 3724–3729, Jul. 2018.

[20] I. Mohamed, Z. Briqech, and A. Sebak, "Antipodal Fermi tapered slot antenna for 60-GHz band applications," *IEEE Antennas Wireless Propag. Lett.*, vol. 14, pp. 96–99, 2015.

[21] R. Harrington and J. Mautz, "Theory of characteristic modes for conducting bodies," *IEEE Trans. Antennas Propag.*, vol. AP-19, no. 5, pp. 622–628, Sep. 1971.

[22] W. Li, Y. Liu, J. Li, L. Ye, and Q. H. Liu, "Modal proportion analysis in antenna characteristic mode theory," *Int. J. Antennas Propag.*, vol. 2019, Feb. 2019, Art. no. 7069230.

[23] C. R. Peñafiel-Ojeda, C. E. Andrade, R. Baez-Egas, and V. Garcia-Santos, "An ultrawideband printed monopole antenna analyzed with the theory of characteristic modes," *IEEE Latin Amer. Trans.*, vol. 20, no. 6, pp. 948–954, Jun. 2022.

[24] W. L. Stutzman and A. T. Gary, *Antenna Theory and Design*. Hoboken, NJ, USA: Wiley, 2012.

[25] Datasheets. (2021). *RFP-DS-Eccosorb AN 180620*. [Online]. Available: https://www.laird.com/

[26] O. Luukkonen et al., "Simple and accurate analytical model of planar grids and high-impedance surfaces comprising metal strips or patches," *IEEE Trans. Antennas Propag.*, vol. 56, no. 6, pp. 1624–1632, Jun. 2008.

[27] S.-W. Lee, G. Zarrillo, and C.-L. Law, "Simple formulas for transmission through periodic metal grids or plates," *IEEE Trans. Antennas Propag.*, vol. AP-30, no. 5, pp. 904–909, Sep. 1982.

[28] D. F. Sievenpiper, *High-Impedance Electromagnetic Surfaces*. Los Angeles, CA, USA: Univ. California, 1999.

[29] D. Sievenpiper, L. Zhang, R. F. J. Broas, N. G. Alexopolous, and E. Yablonovitch, "High-impedance electromagnetic surfaces with a forbidden frequency band," *IEEE Trans. Microw. Theory Techn.*, vol. 47, no. 11, pp. 2059–2074, Nov. 1999.

Ababil Hossain was born in Kushtia, Bangladesh, in 1990. He received the B.Sc. and M.Sc. degrees in electrical and electronic engineering from the Bangladesh University of Engineering and Technology (BUET), Dhaka, Bangladesh, in 2012 and 2015, respectively, the M.S.E.E. degree from Utah State University, Logan, UT, USA, in 2017, and the Ph.D. degree in electrical and computer engineering from University of California at Davis, Davis, CA, USA, in 2023.

He was a Lecturer with the Department of Electrical and Electronic Engineering, Bangladesh University of Business and Technology (BUBT), Dhaka, from 2012 to 2014. He also worked as a Lecturer with the Department of Electronics and Communications Engineering, East West University, Dhaka, in 2018. He worked as an Antenna Engineer with i5 Technologies Inc., Logan, in 2017, for nine months. From 2014 to 2016, he was a Research Assistant at Utah State University. Since 2018, he has been with the Microwave Microsystems Laboratory, University of California at Davis, where he is currently working as a Graduate Student Researcher. His current research interests include electrically compact antennas, ultrawideband (UWB) antennas, phased-array antennas, reconfigurable antennas, metamaterials, radio frequency (RF) circuits, and radar.

Dr. Hossain received the Advancement-to-Candidacy (AC) Fellowship and the Dissertation Writing Fellowship at UC Davis in 2022. He also received the University Undergraduate Admission Test Excellency Scholarship at BUET in 2007 for securing the 14th position. He served as the Session Co-Chair for the IEEE APS/URSI Conference held in Singapore in December 2021.

Anh-Vu Pham (Fellow, IEEE) received the B.E.E. (Hons.), M.S., and Ph.D. degrees in electrical engineering from the Georgia Institute of Technology, Atlanta, GA, USA, in 1995, 1997, and 1999, respectively.

He joined the University of California at Davis, Davis, CA, USA, in 2002, as an Assistant Professor and was promoted to Full Professor in 2008. From 1999 to 2002, he was an Assistant Professor with Clemson University, Clemson, SC, USA. He is currently the Co-Director of the Davis Millimeter Wave Research Center. He is conducting research in RF to THz integrated circuits, antennas, radar and sensors, and energy harvesting systems. His research has been supported by governmental agencies, national laboratories, and companies. He has published over 200 peer-reviewed articles, several book chapters, and two books and has graduated 28 Ph.D. students. In 1997, he cofounded RF Solutions, Atlanta, a fabless RF IC company. In 2003, RF Solutions was acquired by Anadigics, Warren, NJ, USA. In 2008, he cofounded Planarmag, Inc., West Sacramento, CA, USA, and served as the CTO. In 2010, Planarmag, Inc., was acquired by TE Connectivity, Schaffhausen, Switzerland.

Dr. Pham received the National Science Foundation CAREER Award in 2001 and the Outstanding Young Engineer Award from the IEEE Microwave Theory and Techniques Society in 2008. He served as the Co-Chair for the Technical Program Committee (TPC) of the 2016 IEEE International Microwave Symposium (IMS), San Francisco, and the TPC Co-Chair for the 2017 IEEE Asia Pacific Microwave Conference, Malaysia; an IEEE MTT-S Distinguished Microwave Lecturer from 2010 to 2012; and a member/Chair of the IMS Technical Program Review Committee on Power Amplifiers. He served as a Guest Editor for the IEEE TRANSACTIONS ON MICROWAVE THEORY AND TECHNIQUES Special Issues on Broadband Millimeter-Wave Power Amplifiers in 2020 and the Asia-Pacific Microwave Conference in 2017.